Nanofabrication (2022) 7, 325-330
https://doi.org/10.37819/nanofab.007.192

eurasia

SHORT COMMUNICATION

Check for updates

Synthesis, Characterization, and Remedial Action of Biogenic *p*-Ag Nanoparticles

Somya Sinha[1], Belay Zeleke Sibuh[2], Abhilasha Mishra[3], Kumud Pant[1]*, Shikha Tomar[1], Jigisha Anand[1], Piyush Kumar Gupta[1,4]*

[1]*Department of Biotechnology, Graphic Era Deemed to be University, Dehradun 248002, Uttarakhand, India*
[2]*Department of Biotechnology, School of Engineering and Technology, Sharda University, Greater Noida 201310, Uttar Pradesh, India*
[3]*Department of Chemistry, Graphic Era Deemed to be University, Dehradun 248002, Uttarakhand, India*
[4]*Department of Life Science, School of Basic Sciences and Research, Sharda University, Greater Noida 201310, Uttar Pradesh, India*
**Corresponding authors: Dr. Piyush Kumar Gupta (dr.piyushkgupta@gmail.com); Dr. Kumud Pant (pant.kumud@gmail.com).*

ABSTRACT

In the present study, the silver (Ag) nanoparticles (NPs) were fabricated using *pakhoi* (*p*), a traditional alcoholic beverage popularly used in the Garhwal region of Uttarakhand that has been known to possess significant antimicrobial activity properties. Different physicochemical techniques were used to characterize *p*-Ag NPs. The results confirm the synthesis of crystalline *p*-Ag NPs having a nearly spherical shape with a net positive charge. Further, *p*-Ag NPs exhibit strong antibacterial activity against Gram -ve bacteria. Moreover, a detailed study will be beneficial to understanding and exploiting the biomedical application and environmental remediation activity of the *p*-Ag NPs.

ARTICLE HISTORY

Received: 16-03-2022
Revised: 5-04-2022
Accepted: 7-05-2022

KEYWORDS

Antibacterial
Green synthesis
Pakhoi
Silver nanoparticles

1. Introduction

The synthesis of NPs is majorly carried out using several chemical approaches that are non-eco-friendly and expensive processes. Over the past decade, nanotechnologists have broadened their research on the synthesis of metal NPs due to their looming applications. Recently, metal NPs have been extensively used in biomedical and environmental remediation applications [1–5]. These metal NPs include Fe, Zn, Cu, Si, Ag, Au, Ni, etc. Among these metallic NPs, both silver (Ag) and gold (Au) NPs showed their more extensive use in medicine as an antibacterial, antifungal, anticancer, and anti-inflammatory agents as well as in biosensing, bioelectronic, and photocatalytic applications [6–8]. Further, Ag NPs are among the most studied NP due to their excellent stability and good catalytic activity in various redox reactions. The biogenic Ag NPs also exhibited potent antibacterial activity against different human bacterial pathogens [9].

In the meantime, the green synthesis of metal NPs is being considered a bottom-up approach that is absolutely environment friendly and does not require the practice of any toxic chemicals or organic solvents. While it mainly uses the aqueous extracts obtained from various biological resources such as plants, fungus, bacteria, algae, and protists,

thereby making the green synthesis approach more sustainable and eco-friendly [10–15]. However, one major problem arises during the fabrication of plant extract-based metal NPs, i.e., the variation in the concentration of bioactive compounds or phytoconstituents, which differs according to the geographical location of the desired plant. The method adopted in the present work does not involve using expensive organic solvents, nor does it rely on the isolation technique or any culture preparation like other green synthesis approaches. Owing to the cost-efficacy and sustainable production, the present study follows a bottom-up approach by utilizing *pakhoi,* a renowned traditional beverage of Uttarakhand state since ancient times to prepare Ag NPs without relying on extract preparation. The fabricated *p*-Ag NPs are physiochemically characterized via FTIR, XRD, DLS, and HR-TEM instruments, and finally, their antibacterial properties were evaluated against gram – ve bacterial pathogen.

2. Materials and Methodology

2.1 Preparation of Pakhoi

Pakhoi sample was collected from the Garhwal region of Uttarakhand (77° 49′-78° 37' E longitude and 30° 35′-30° 18' N latitude). The sample was filtered using Whatman filter paper, and the obtained filtrate was centrifuged at 4000 rpm for 10 minutes. After centrifugation, the collected supernatant was kept in the refrigerator until further use.

2.2 Fabrication of *p*-Ag nanoparticles

Initially, 1 mM aqueous solution of silver nitrate ($AgNO_3$) was prepared under dark conditions. Next, 5mL of 1 mM $AgNO_3$ solution added separately to the varying volume (1 mL, 2 mL, 3 mL, 4 mL, 5 mL) of the *pakhoi* sample. The resulting mixtures were further diluted with distilled water to make a final volume of 10 mL to get the final 0.5 mM concentration of $AgNO_3$. The diluted reaction mixtures were kept for five days in the dark and finally confirmed the reduction of Ag^1 to Ag^0 by seeing a variation in the color of solutions (Figure 1a).

2.3 Physicochemical characterizations of *p*-Ag nanoparticles

UV/Visible spectrophotometer (UV/Vis 10 Spectroscopy, Thermo Scientific) was used to study the formation of *p*-Ag NPs. The fabricated *p*-Ag NPs were diluted ten times using distilled water and then scanned between 300 and 450 nm to obtain the maximum absorbance wavelength (λ_{max}). Next, the NANOTRAC Wave II/Q/Zeta instrument was used to calculate the average hydrodynamic size ($\mathbf{Z_{Average}}$) and average zeta potential of *p*-Ag NPs during the dynamic light scattering (DLS) experiment. FTIR spectroscopy (FTIR-6800, JASCO) examined various bridging functional group linkages of different bioactive compounds (present in the *pakhoi* sample) with Ag NPs. The vibrational peaks of other functional groups were recorded between 400 and 4000 cm^{-1}. Further, an X-ray diffractometer (XRD) was used to analyze the crystal lattice structure of *p*-Ag NPs. The range of diffraction angles was taken between 10 and 80°. In last, High-Resolution Transmission Electron Microscopy (HRTEM) instrument (Tecnai) was used to examine the morphology and size of *p*-Ag NPs. The selected area electron diffraction (SAED) pattern was used to analyze the structure of *p*-Ag NPs [16].

2.4 Antibacterial activity

Escherichia coli (MTCC 42) culture was used for the antibacterial test. The obtained bacteria were cultured and sub-cultured in Luria Bertani (LB) media to bring the pure bacterial colonies. The antibacterial test was carried out via the agar well diffusion method. In brief, 100 µL of overnight grown *E. coli* culture was aseptically transferred on the agar surface of Mueller Hinton Agar medium plates and gently spread using a glass spreader. Then, eight wells of 6 mm diameter were created in the same plate where five wells were used for five different concentrations of *p*-Ag NPs (NP1 – NP5), one well for the positive control (Ampicillin – 100 µg/mL), one well for *pakhoi*, and one well for $AgNO_3$ solution alone. The test was done in duplicates. Subsequently, the test plates were incubated overnight at 37°C for 24 h. Later, the diameter for the zone of inhibition (in mm) was measured.

2.5 Statistical analysis

All the experiments were carried out three independent times. The obtained data were analyzed using Origin 8 software.

Results and Discussion

3.1 Fabrication of *p*-Ag nanoparticles

The *p*-Ag NPs were fabricated by observing a variation in the color of the reaction mixture. When the volume of the *pakhoi* sample (1 – 5 mL) was increased into $AgNO_3$ solution (1 mM), then the changes were seen in the color of different reaction mixtures (NP1 – NP5) from light brown to dark brown (Figure 1a). The obtained colloidal brown color indicates the formation of *p*-Ag NPs.

3.2 Physicochemical characterizations

UV-Visible spectral analysis displayed the reduction of Ag^+ ions into Ag^0 NPs. The highest absorbance peaks of different *p*-Ag NPs (NP1 – NP5) were observed between 405 – 420 nm that exhibited a surface plasmon resonance (SPR) signature for the fabrication of *p*-Ag NPs [9] (Figure 1b). It was also observed that the absorbance of *p*-Ag NPs rises with an increase in the volume of added *pakhoi* sample (Figure 1b). It might be due to the formation of more *p*-Ag NPs at a higher volume of *pakhoi* samples. Next, the DLS experiment was used to calculate the average hydrodynamic size of *p*-Ag NPs (NP2) which was calculated to be maximum at 49.9 and 159 d.nm (Figure 1c). The average zeta potential was calculated to be + 23.8 ± 0.3 mV. Further, the crystalline nature of *p*-Ag NPs (NP2) was confirmed by XRD. The diffraction peaks of *p*-Ag NPs were observed at 2θ values of 38.19°, 44.31°, 64.50°, and 77.41°, corresponding to (111), (200), (220) and (311) Bragg reflections, respectively indicating the face-centered cubic structure of Ag crystals (Figure 1d). The obtained diffraction peaks matched with Ag XRD ref. no. 01-087-0719. The unassigned diffraction peak (*) at 26.45° might be related to the amorphous organic phase (Figure 1d). The average crystallite size of *p*-Ag NPs (NP2) was calculated at 29 nm using Scherrer's formula [9]. Furthermore, the FTIR spectrum of p-Ag NPs (NP2) demonstrated the functional molecules on the NP's surface. The intent peaks at 1261.21 cm^{-1}, 1081.17 cm^{-1}, and 1024.01 cm^{-1} were assigned to the C-O stretching. The peaks at 3381.56 cm^{-1} and 872.63 cm^{-1} were assigned to the O-H stretching and bending. The C-H stretching was seen at the peak range of 2935.21 cm^{-1}, and C=C stretching was observed at 1614.12 cm^{-1} and 1426.10 cm^{-1}. The out-of-plane C-H and O-H bending appeared at 714.49 cm^{-1} and 630.60 cm^{-1}. The obtained FTIR spectrum indicated that various functional molecules capped the prepared p-AgNPs. In addition, HR-TEM was used to study the shape of *p*-Ag NPs (NP2) that was observed to be nearly spherical (Figure 2a, b). SAED pattern of *p*-Ag NPs (NP2)

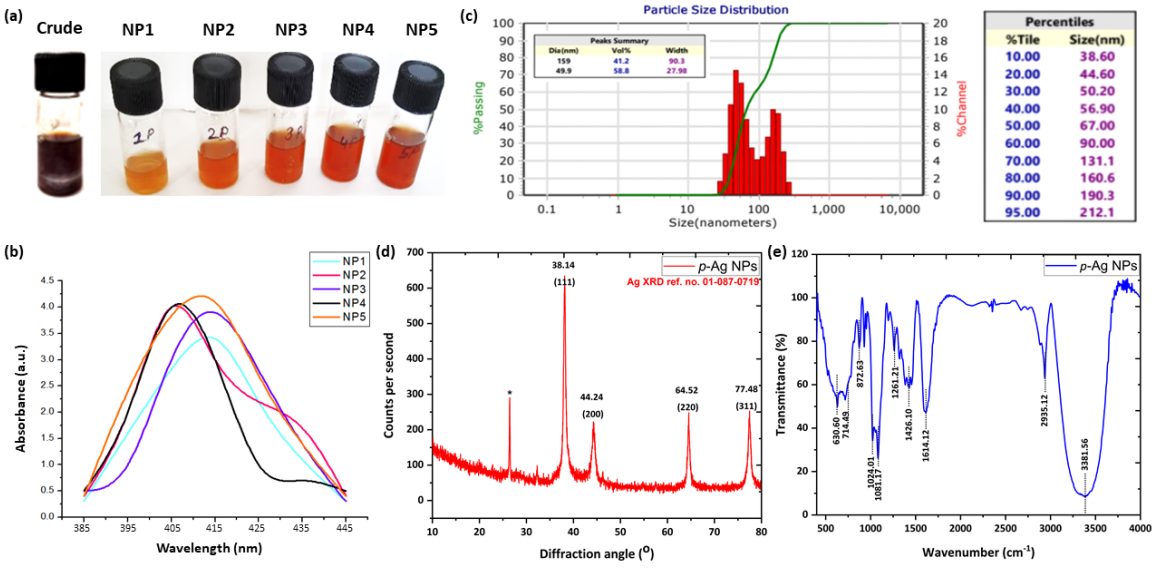

Figure 1. **(a)** Crude extract of *pakhoi* and images of different *p*-Ag NPs (NP1–NP5) fabricated with the varying volume of *pakhoi* sample, **(b)** UV-Visible spectrum of different *p*-Ag NPs (NP2), **(c)** particle size distribution, **(d)** XRD pattern, and **(e)** FTIR spectrum of *p*-Ag NPs (NP2).

showed the concentric rings with intermittent dots indicating the crystalline nature of *p*-Ag NPs [17].

3.3 Antibacterial activity

The antibacterial activity of *p*-Ag NPs (NP1 – NP5) was tested on *E. coli,* and the resulting MIC values were summarized in a tabulated form (Figure 2d). No significant difference was observed in the zone of inhibition (ZoI) values of different *p*-Ag NPs (NP1 – NP5). However, *p*-Ag NPs displayed a potent antibacterial activity compared to the *pakhoi* sample and $AgNO_3$ solution (Figure 2e), which can be seen with significant differences in their ZoI values (Figure 2d). A previous study showed that Ag NPs possess a larger surface area that improves their interactions with bacteria cell wall components. Also, the positively charged Ag NPs interact with negatively charged bacterial cells responsible for the antibacterial activity [9,17]. In 2021, Naveen *et al.* fabricated Pc-Ag NPs using the aqueous leaf extracts of *Potentilla chinensis* Ser. These NPs inhibited the growth of gram + ve and gram – ve bacteria like *E. coli, Bacillus cereus, Staphylococcus aureus and salmonella enterica* [11]. Next, in 2021, Chowdhury *et al.* isolated an antimicrobial compound Tridecanoic acid, from *Bacillus sp*. This purified compound synthesised and stabilised Ag NPs that showed strong antibacterial and antifungal activities against human and plant pathogens [18]. Further, many studies previously reported the photocatalytic activity of Ag NPs in removing both organic and inorganic pollutants from wastewater. Similarly, in 2021, Lotfollahzadeh *et al.* used the aqueous extract of *Oenothera biennis* to fabricate Ag NPs for the removal of amoxicillin from wastewater. The prepared Ag NPs showed the potent antibacterial activity against *S. aureus* and *E. coli* bacteria. Also, 97.27 % removal efficiency was seen for amoxicillin by Ag NPs in 30 min [4]. However, the biogenic Ag NPs also possess other biological activities like anticancer, anti-inflammatory, anti-leishmanial, and anti-viral. In 2021, Chandan *et al.* synthesized Ag NPs using the leaves of *Datura stramonium.* These NPs exhibited potent anticancer activity against various cancers like pancreatic (PANC-1), colon (HCT 116), lung (A549), and brain cancers (U87, SH-SY5Y) [19].

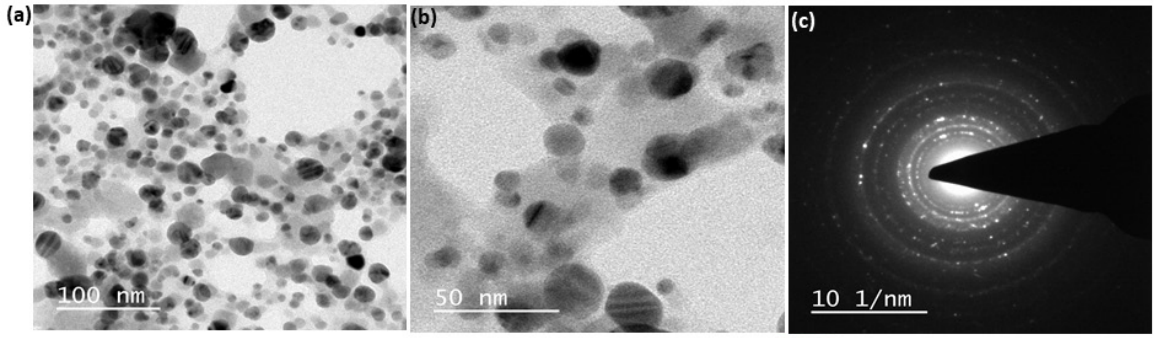

(d)

Tested Sample	ZoI Values (mm)
Positive Control	3.3
Pakhoi	0.1
$AgNO_3$	0.2
NP1	1.3
NP2	1.4
NP3	1.3
NP4	1.4
NP5	1.3

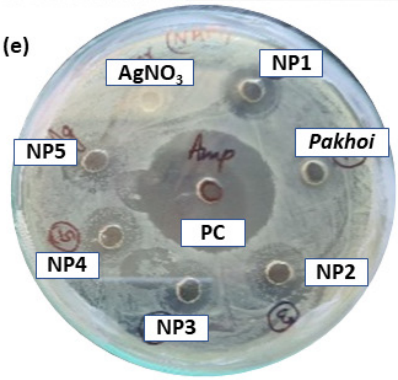

Figure 2. **(a, b)** HR-TEM images of *p*-Ag NPs (NP2) on different magnifications, **(c)** SAED pattern of *p*-Ag NPs (NP2), **(d)** ZoI values of different *p*-Ag NPs (NP1-NP5) along with positive control, *pakhoi*, and $AgNO_3$ solution shown in tabulated form, and **(e)** antibacterial test of tested samples using agar well diffusion method.

4. Conclusion

The green synthesis approach is highly cost-effective and environmentally friendly for NP synthesis. This study fabricated *p*-Ag NPs using a *pakhoi* sample. The UV/Visible spectrophotometer exhibited the formation of *p*-Ag NPs. HR-TEM analysis displayed the nearly spherical shape of *p*-Ag NPs. Further, both XRD and SAED patterns showed the crystalline nature of *p*-Ag NPs. The DLS analysis confirmed the nano-size of *p*-Ag NPs, and the net positive charge was present on NP's surface. Next, FTIR analysis indicated the presence of different functional groups on NP's surface. Later, *p*-Ag NPs exhibited strong antibacterial activity against *E. coli* bacteria. The p-Ag NPs can be used soon for biomedical and environmental remediation applications based on these results.

Acknowledgment

Dr Piyush Kumar Gupta is thankful to the Department of Life Science, School of Basic Sciences and Research, Sharda University and the Department of Biotechnology, Graphic Era Deemed to be University for providing the infrastructure and research facilities.

Conflicts of interest

All authors have no competing interests to declare relevant to this article's content.

Funding

The authors did not receive funding from any organization for the submitted work.

References

1. Riva L, Pastori N, Panozzo A, Antonelli M, Punta C. Nanostructured Cellulose-Based Sorbent Materials for Water Decontamination from Organic Dyes. Nanomaterials [Internet]. 2020 Aug 10;10(8):1570. Available from: https://www.mdpi.com/2079-4991/10/8/1570
2. Singh P, Kaur N, Khunger A, Kaur G, Kumar S, Kaushik A, *et al.* Green-monodispersed Pd-nanoparticles for improved mitigation of pathogens and environmental pollutant. Mater Today Commun [Internet]. 2022 Mar 1 [cited 2022 Mar 22];30:103106. Available from: https://linkinghub.elsevier.com/retrieve/pii/S2352492821010904
3. Tiwari S, Juneja S, Ghosal A, Bandara N, Khan R, Wallen SL, *et al.* Antibacterial and antiviral high-performance nanosystems to mitigate new SARS-CoV-2 variants of concern. Curr Opin Biomed Eng [Internet]. 2022 Mar 1 [cited 2022 Mar 22];21:100363. Available from: https://linkinghub.elsevier.com/retrieve/pii/S2468451121001033
4. Lotfollahzadeh R, Yari M, Sedaghat S, Delbari AS. Biosynthesis and characterization of silver nanoparticles for the removal of amoxicillin from aqueous solutions using Oenothera biennis water extract. J Nanostructure Chem [Internet]. 2021;11(4):693–706. Available from: https://doi.org/10.1007/s40097-021-00393-x
5. Frenzilli G. Nanotechnology for Environmental and Biomedical Research. Nanomaterials [Internet]. 2020 Nov 8;10(11):2220. Available from: https://www.mdpi.com/2079-4991/10/11/2220
6. Hosny M, Eltaweil AS, Mostafa M, El-Badry YA, Hussein EE, Omer AM, *et al.* Facile Synthesis of Gold Nanoparticles for Anticancer, Antioxidant Applications, and Photocatalytic Degradation of Toxic Organic Pollutants. ACS Omega [Internet]. 2022 Jan 25;7(3):3121–33. Available from: https://pubs.acs.org/doi/10.1021/acsomega.1c06714
7. Desalegn T, Ravikumar CR, Murthy HCA. Eco-friendly synthesis of silver nanostructures using medicinal plant Vernonia amygdalina Del. leaf extract for multifunctional applications. Appl Nanosci [Internet]. 2021;11(2):535–51. Available from: https://doi.org/10.1007/s13204-020-01620-7
8. Urnukhsaikhan E, Bold BE, Gunbileg A, Sukhbaatar N, Mishig-Ochir T. Antibacterial activity and characteristics of silver nanoparticles biosynthesized from Carduus crispus. Sci Rep [Internet]. 2021;11(1):1–12. Available from: https://doi.org/10.1038/s41598-021-00520-2
9. Kumar Gupta P, Karthik Kumar D, Thaveena M, Pandit S, Sinha S, Ranjithkumar R, *et al.* Synthesis, Characterization and Remedial Action of Biogenic Silver Nanoparticles and Chitosan-Silver Nanoparticles against Bacterial Pathogens. J Renew Mater

[Internet]. 2022;10(5):1–13. Available from: https://www.techscience.com/jrm/online/detail/18318

10. Krishnan S, Patel PN, Balasubramanian KK, Chadha A. Yeast supported gold nanoparticles: an efficient catalyst for the synthesis of commercially important aryl amines. New J Chem [Internet]. 2021;45(4):1915–23. Available from: http://xlink.rsc.org/?DOI=D0NJ04542J
11. Naveen KV, Kim H-Y, Saravanakumar K, Mariadoss AVA, Wang M-H. Phyto-fabrication of biocompatible silver nanoparticles using Potentilla chinensis Ser leaves: characterization and evaluation of its antibacterial activity. J Nanostructure Chem [Internet]. 2021; Available from: https://doi.org/10.1007/s40097-021-00439-0
12. Win TT, Khan S, Bo B, Zada S, Fu P. Green synthesis and characterization of Fe3O4 nanoparticles using Chlorella-K01 extract for potential enhancement of plant growth stimulating and antifungal activity. Sci Rep [Internet]. 2021 Dec 9;11(1):21996. Available from: https://www.nature.com/articles/s41598-021-01538-2
13. Faisal S, Jan H, Shah SA, Shah S, Khan A, Akbar MT, *et al.* Green Synthesis of Zinc Oxide (ZnO) Nanoparticles Using Aqueous Fruit Extracts of Myristica fragrans : Their Characterizations and Biological and Environmental Applications. ACS Omega [Internet]. 2021 Apr 13;6(14):9709–22. Available from: https://pubs.acs.org/doi/10.1021/acsomega.1c00310
14. Vinodhini S, Vithiya BSM, Prasad TAA. Green synthesis of silver nanoparticles by employing the Allium fistulosum, Tabernaemontana divaricate and Basella alba leaf extracts for antimicrobial applications. J King Saud Univ - Sci [Internet]. 2022;34(4):101939. Available from: https://doi.org/10.1016/j.jksus.2022.101939
15. Algotiml R, Gab-Alla A, Seoudi R, Abulreesh HH, El-Readi MZ, Elbanna K. Anticancer and antimicrobial activity of biosynthesized Red Sea marine algal silver nanoparticles. Sci Rep [Internet]. 2022;12(1):1–18. Available from: https://doi.org/10.1038/s41598-022-06412-3
16. Chabattula SCC, Gupta PKK, Tripathi SKK, Gahtori R, Padhi P, Mahapatra S, *et al.* Anticancer therapeutic efficacy of biogenic Am-ZnO nanoparticles on 2D and 3D tumor models. Mater Today Chem [Internet]. 2021 Dec;22:100618. Available from: https://doi.org/10.1016/j.mtchem.2021.100618
17. Venugopal K, Rather HA, Rajagopal K, Shanthi MP, Sheriff K, Illiyas M, *et al.* Synthesis of silver nanoparticles (Ag NPs) for anticancer activities (MCF 7 breast and A549 lung cell lines) of the crude extract of Syzygium aromaticum. J Photochem Photobiol B Biol [Internet]. 2017 Feb;167:282–9. Available from: http://dx.doi.org/10.1016/j.jphotobiol.2016.12.013
18. Chowdhury SK, Dutta T, Chattopadhyay AP, Ghosh NN, Chowdhury S, Mandal V. Isolation of antimicrobial Tridecanoic acid from Bacillus sp. LBF-01 and its potentialization through silver nanoparticles synthesis: a combined experimental and theoretical studies. J Nanostructure Chem [Internet]. 2021;11(4):573–87. Available from: https://doi.org/10.1007/s40097-020-00385-3
19. Chandan G, Pal S, Kashyap S, Siwal SS, Dhiman SK, Saini AK, *et al.* Synthesis, characterization and anticancer activities of silver nanoparticles from the leaves of Datura stramonium L. Nanofabrication. 2021;6(1):25–35.